

## Chapter 2

# Interacting Dirac Fermions in (3+1) Dimensions

**Abstract** The long-range electron-electron interaction between Dirac electrons in  $(3 + 1)$  dimensions is considered by the perturbative renormalization group analysis. When the chemical potential in Dirac energy dispersion is tuned at the band crossing point, the density of states vanishes and hence the Coulomb interaction is not screened to become a long-range force. We analyze that long-range interaction relativistically, taking into consideration of the retardation effect of the propagation of the interaction. Those massless Dirac electrons in  $(3 + 1)$  dimensions emerge, for example, at the quantum critical point of topological phase transitions and in Weyl/Dirac semimetals. They receive logarithmic corrections in the nonrelativistic regime, where the electron's speed  $v$  is much larger than the speed of light  $c$ ;  $v$  increases logarithmically depending on the renormalization scale. In the low energies, however, the Dirac systems attain a relativistic regime  $v \approx c$ , and finally the Lorentz invariance is recovered ( $v = c$ ).

**Keywords** Dirac fermions · Dirac/Weyl semimetals · Electron-electron interaction · Renormalization group · Lorentz invariance

In solids, the electronic states are described by the Bloch wave functions with the energy dispersion  $\varepsilon_n(\mathbf{k})$ , where  $n$  is a band index and  $\mathbf{k}$  is crystal momentum. The velocity of electrons given by  $\mathbf{v}_n(\mathbf{k}) = \partial \varepsilon_n(\mathbf{k}) / \partial \mathbf{k}$  is usually much smaller than that of light  $c$ . Therefore, the Lorentz invariance is terribly broken and hence many of the beautiful results in QED [1, 2] are not applicable to the Bloch electrons in solids. The smallness of the factor  $v_n(\mathbf{k})/c \ll 1$  naturally leads to the gauge choice (i.e., Coulomb gauge), where the scalar potential gives the Coulomb interaction without retardation while the electron-electron interaction through the transverse part of the vector potential  $\mathbf{A}$  is often neglected. The latter is often treated as the external electromagnetic field for the probe of the electromagnetic response of the system. This gauge choice is regarded as “physical gauge.” For example, one can discuss the physical meaning of the Green's function  $G(\mathbf{k}, \omega)$  in this gauge, where the quasiparticle corresponds its pole structure. ARPES is also formulated in this gauge, i.e., ARPES intensity is proportional to the electron spectrum function  $-\text{Im}G(\mathbf{k}, \omega)$  [3].

The effects of electron-electron interaction on the Dirac electrons are extensively studied [4–7]. For graphene, it has been revealed that the electron speed  $v$  is

renormalized to increase logarithmically by the long-range Coulomb interaction, while the coupling constant  $\alpha$  is marginally irrelevant [4]. When the exchange of the transverse part of the vector potential is taken into account, the velocity  $v$  saturates to that of light  $c$  (i.e., the Lorentz invariance is recovered) and  $\alpha$  remains finite in the infrared limit. This leads to an intriguing non-Fermi liquid state in (2+1) dimensions [5]. The quantum critical behavior close to the superconducting transition is also studied [8]. For (3+1)D massless Dirac systems, the Coulomb interaction also gives the logarithmic enhancement of the velocity  $v$  and the coupling constant  $\alpha$  is marginally irrelevant [6, 7]. The disorder potential is irrelevant perturbatively, while strong enough disorder drives the system toward the compressible diffusive metal [6, 9].

In this chapter, we study the effects of electron-electron interaction on Dirac (or Weyl) electrons in (3+1) dimensions using RG analysis. The quantum critical phenomena of topological phase transition and Weyl semimetals are considered as physical realizations of such systems. The Coulomb interaction as well as the transverse current-current interaction are considered in the following analysis.

## 2.1 Model

We start with the following Lagrangian<sup>1</sup>:

$$\mathcal{L} = \bar{\psi}_a(\gamma^0 p_0 - v\boldsymbol{\gamma} \cdot \mathbf{p} - m)\psi_a + \frac{1}{2}(\varepsilon \mathbf{E}^2 - \frac{1}{\mu} \mathbf{B}^2) - e\bar{\psi}_a l_\nu^\mu \gamma^\nu \psi_a A_\mu, \quad (2.1)$$

where  $\psi_a$  is a four-component Dirac spinor with  $a$  being the  $N$  flavor index, and the matrix

$$l_\nu^\mu = \begin{pmatrix} 1 & & & \\ & v/c & & \\ & & v/c & \\ & & & v/c \end{pmatrix} \quad (2.2)$$

is defined to describe the electromagnetic interactions in a system without Lorentz invariance. We use the Lorentzian metric defined by the metric tensor  $g^{\mu\nu} = \text{diag}(1, -1, -1, -1)$ . To separate the temporal and spatial components, we introduce a spatial index  $\alpha = 1, 2, 3$  and  $\gamma^\alpha p_\alpha = -\boldsymbol{\gamma} \cdot \mathbf{p}$ . For the moment, we consider a

---

<sup>1</sup>We have dropped the  $\theta$  term, i.e.,  $\theta \mathbf{E} \cdot \mathbf{B}$  ( $\theta = \pm\pi$ ) in the action, which should be present in the TI phase. This term, however, can be transformed into the surface term, and the sign of  $\theta$  is determined by the time-reversal symmetry breaking on the surface [10]. The topological magnetoelectric effect is derived from this term, but this is beyond the scope of this present analysis, where only the bulk properties are discussed.

Actually, the RG analysis does not modify the  $\theta$  term. It is natural since topological terms have discrete integer values, and we confirmed this fact from the following two methods: the perturbative calculation and the background field theory. In any case, the topological  $\theta$  term does not alter the bulk properties.

massless case, i.e.,  $m = 0$ , which corresponds to quantum critical phenomena of TIs and Weyl semimetals. The renormalization of the mass  $m$  will be discussed later.

If we consider massless Weyl nodes, the Lagrangian has the chiral symmetry, and the four-component Dirac spinor can be separated into two two-component Weyl spinors with opposite chiralities. Thus, the number of Weyl nodes  $N_W$  are twice as large as that of Dirac nodes  $N$ , i.e.,  $N_W = 2N$ . In the following analysis, we treat the model in the four-component notation. If necessary, we can use the projection operators  $(1 \pm \gamma^5)/2$  to separate the Dirac fermion into two Weyl fermions with opposite chiralities.

The speed of light in material  $c$  and in vacuum  $c_{\text{vacuum}} = 3 \times 10^8$  m/s are related through the permittivity  $\varepsilon$  and the permeability  $\mu$  by  $c^2 = c_{\text{vacuum}}^2/(\varepsilon\mu)$ . The electric field and magnetic field are represented in terms of the photon field  $A_\mu$  as

$$\mathbf{E} = -\frac{1}{c} \frac{\partial \mathbf{A}}{\partial t} - \nabla A_0, \quad \mathbf{B} = \frac{1}{c} \nabla \times \mathbf{A}. \quad (2.3)$$

The electron propagator  $G_0(p)$ , the photon propagator  $D_0^{\mu\nu}(p)$ , and the vertex  $\Gamma_0^\mu$  are given by

$$G_0(p) = \frac{i}{\gamma^0 p_0 + v \gamma^\alpha p_\alpha + i0}, \quad (2.4)$$

$$D_0^{\mu\nu}(q) = \frac{-ic^2 g^{\mu\nu}}{\varepsilon(q_0^2 - c^2 q_\alpha^2) + i0}, \quad (2.5)$$

$$\Gamma_0^\mu = -ie l_\nu^\mu \gamma^\nu = \left( -ie \gamma^0, -ie \frac{v}{c} \gamma^\alpha \right). \quad (2.6)$$

Here we employ the Feynman gauge because physical quantities are independent of gauge choice.

## 2.2 Renormalization Group Analysis

### 2.2.1 Perturbative Calculation

Calculations are performed by using dimensional regularization [11] not to violate the gauge invariance of the theory. We set the spacetime dimension  $d = 4 - \epsilon$  to regularize divergences. The self-energy  $\Sigma_2(p)$ , polarization  $\Pi_2^{\mu\nu}(q)$ , and the vertex correction  $\delta\Gamma^\mu(p', p)$  are calculated to one-loop order (Fig. 2.1).

First, we consider the one-loop self-energy contribution (Fig. 2.1a). According to the Feynman rule, this diagram is calculated by

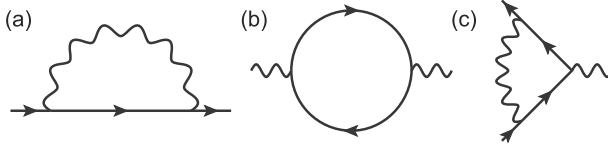


**Fig. 2.1** One-loop Feynman diagrams considered in the analysis: **a** self-energy, **b** polarization, **c** vertex. Reprinted figure with permission from Ref. [12]. Copyright 2012 by the American Physical Society

$$\begin{aligned}
 & -i\Sigma_2(p) \\
 &= (-ie)^2 \int \frac{d^d k}{(2\pi)^d} \gamma^0 \frac{i(\gamma^0 k_0 - v\gamma \cdot \mathbf{k})}{k_0^2 - v^2 \mathbf{k}^2} \gamma^0 \frac{-ic^2}{\varepsilon[(p_0 - k_0)^2 - c^2(\mathbf{p} - \mathbf{k})^2]} \\
 &+ (-ie)^2 \left(\frac{v}{c}\right)^2 \int \frac{d^d k}{(2\pi)^d} \gamma^\alpha \frac{i(\gamma^0 k_0 - v\gamma \cdot \mathbf{k})}{k_0^2 - v^2 \mathbf{k}^2} \gamma_\alpha \frac{-ic^2}{\varepsilon[(p_0 - k_0)^2 - c^2(\mathbf{p} - \mathbf{k})^2]}. \quad (2.7)
 \end{aligned}$$

After performing the momentum integrals in  $(4 - \epsilon)\text{D}$  space, we obtain the one-loop self-energy

$$\Sigma_2(p) = \frac{g^2}{\pi\epsilon} \frac{c}{(c+v)^2} \left[ 1 - 3\left(\frac{v}{c}\right)^2 \right] \gamma^0 p_0 + \frac{g^2}{3\pi\epsilon} \frac{(2c+v)c}{(c+v)^2 v} \left[ 1 + \left(\frac{v}{c}\right)^2 \right] v\gamma \cdot \mathbf{p}. \quad (2.8)$$

For simplicity, we define the effective charge  $g$  as

$$g^2 = \frac{e^2}{4\pi\varepsilon}. \quad (2.9)$$

Next we consider the polarization (Fig. 2.1b), which is given by

$$\begin{aligned}
 & i\Pi_2^{\mu\nu}(q) \\
 &= (-1)N(-ie)^2 \left(\frac{v}{c}\right)^{2-\delta_{\mu 0}-\delta_{\nu 0}} \\
 &\times \int \frac{d^d k}{(2\pi)^2} \text{tr} \left[ \gamma^\mu \frac{i(\gamma^0 k_0 - v\gamma \cdot \mathbf{k})}{k_0^2 - v^2 \mathbf{k}^2} \gamma^\nu \frac{i(\gamma^0(k_0 + q_0) - v\gamma \cdot (\mathbf{k} + \mathbf{q}))}{(k_0 + q_0)^2 - v^2(\mathbf{k} + \mathbf{q})^2} \right]. \quad (2.10)
 \end{aligned}$$

The factor  $(-1)$  on the right-hand side comes from the fermion loop, and  $N$  is the number of Dirac fermion species. Actually, the polarization is almost the same as that in QED, except the existence of the coefficient  $(v/c)^{2-\delta_{\mu 0}-\delta_{\nu 0}}$ . Evaluating the trace of the gamma matrices and integrating over momentum space gives

$$\Pi_2^{\mu\nu}(q) = (q^2 g^{\mu\nu} - q^\mu q^\nu) \left(\frac{v}{c}\right)^{2-\delta_{\mu 0}-\delta_{\nu 0}} \frac{1}{v^3} N \Pi_2(q), \quad (2.11)$$

where

$$\Pi_2(q) = -\frac{e^2}{6\pi^2\epsilon} + O(\epsilon^0),$$

and  $q^\mu = (q^0, vq^\alpha)$  is an electron four-vector.

The remaining diagram we should evaluate is the vertex function (Fig. 2.1c):

$$\begin{aligned} \delta\Gamma^\mu(p', p) = & \left(\frac{v}{c}\right)^{3-\delta_{\mu 0}-2\delta_{\nu 0}} \int \frac{d^d k}{(2\pi)^d} \frac{-ic^2}{\varepsilon[(k_0 - p_0)^2 - c^2(\mathbf{k} - \mathbf{p})^2]} (-ie\gamma^\nu) \\ & \times \frac{i(\gamma^0 k'_0 - v\boldsymbol{\gamma} \cdot \mathbf{k}')}{k_0'^2 - v^2 \mathbf{k}'^2} \gamma^\mu \frac{i(\gamma^0 k_0 - v\boldsymbol{\gamma} \cdot \mathbf{k})}{k_0^2 - v^2 \mathbf{k}^2} (-ie\gamma_\nu), \end{aligned} \quad (2.12)$$

where  $k' = k + p' - p$ . The vertex function for the temporal and spatial components are calculated separately, and we obtain

$$\delta\Gamma^0(0, 0) = -\frac{g^2}{\pi\epsilon} \frac{c}{(c+v)^2} \left[1 - 3\left(\frac{v}{c}\right)^2\right] \gamma^0, \quad (2.13)$$

$$\delta\Gamma^\alpha(0, 0) = \frac{g^2}{3\pi\epsilon} \frac{(2c+v)c}{(c+v)^2 v} \left[1 + \left(\frac{v}{c}\right)^2\right] \frac{v}{c} \gamma^\alpha. \quad (2.14)$$

## 2.2.2 Renormalization

The diverging quantities appearing in the calculation of the one-loop diagrams are absorbed by adding counterterms and rescaling some quantities. We can write the renormalized Lagrangian  $\mathcal{L}_{\text{ren}}$  in the form

$$\mathcal{L}_{\text{ren}} = \mathcal{L}_0 + \mathcal{L}_{\text{c.t.}}, \quad (2.15)$$

where  $\mathcal{L}_0$  is the original Lagrangian and  $\mathcal{L}_{\text{c.t.}}$  is the counterterm Lagrangian. The counterterms are defined to make the theory finite at a momentum scale  $\kappa_0$ . The parameter  $\kappa_0$  is called the *renormalization scale*, which we discuss in detail in Sect. 2.5.1. In our case, the renormalization scale  $\kappa_0$  corresponds to the cutoff momentum scale.

By defining some new fields and parameters, the renormalized Lagrangian is

$$\begin{aligned} \mathcal{L}_{\text{ren}} = & \bar{\psi}(Z_{2t}\gamma^0 p_0 + Z_{2s}v\gamma^\alpha p_\alpha)\psi + \frac{1}{2}\left(Z_{3e}\varepsilon\mathbf{E}^2 - Z_{3m}\frac{1}{\mu}\mathbf{B}^2\right) \\ & - Z_{1t}e\bar{\psi}\gamma^0\psi A_0 - Z_{1s}e\frac{v}{c}\bar{\psi}\boldsymbol{\gamma}\psi\mathbf{A} \end{aligned}$$

$$\begin{aligned}
&= \bar{\psi}_B(\gamma^0 p_0 + v_B \gamma^\alpha p_\alpha) \psi_B + \frac{1}{2} \left( \varepsilon_B \mathbf{E}_B^2 - \frac{1}{\mu_B} \mathbf{B}_B^2 \right) \\
&\quad - e_B \bar{\psi}_B \gamma^0 \psi_B (A_0)_B - e_B \frac{v_B}{c_B} \bar{\psi}_B \gamma^\alpha \psi_B (A_\alpha)_B.
\end{aligned} \tag{2.16}$$

The subscript B denotes the bare value for each quantity. Each of the field strength renormalization  $Z$  is determined from the one-loop results [Eqs. (2.8), (2.11), (2.13), and (2.14)] to order  $g^2$ . At order  $g^2$ , only divergent terms are retained and finite terms are ignored, since the finite terms have no effect in the RG calculation. The results are

$$Z_{1t} = 1 + \frac{g^2}{\pi\epsilon} \frac{c}{(c+v)^2} \left[ 1 - 3 \left( \frac{v}{c} \right)^2 \right], \tag{2.17}$$

$$Z_{1s} = 1 - \frac{g^2}{3\pi\epsilon} \frac{(2c+v)c}{(c+v)^2 v} \left[ 1 + \left( \frac{v}{c} \right)^2 \right], \tag{2.18}$$

$$Z_{2t} = 1 + \frac{g^2}{\pi\epsilon} \frac{c}{(c+v)^2} \left[ 1 - 3 \left( \frac{v}{c} \right)^2 \right], \tag{2.19}$$

$$Z_{2s} = 1 - \frac{g^2}{3\pi\epsilon} \frac{(2c+v)c}{(c+v)^2 v} \left[ 1 + \left( \frac{v}{c} \right)^2 \right], \tag{2.20}$$

$$Z_{3e} = 1 - \frac{2Ng^2}{3\pi\epsilon} \frac{1}{v}, \tag{2.21}$$

$$Z_{3m} = 1 - \frac{2Ng^2}{3\pi\epsilon} \frac{v}{c^2}. \tag{2.22}$$

Here we can confirm  $Z_{1t} = Z_{2t}$  and  $Z_{1s} = Z_{2s}$ . These relations are consequences of the Ward–Takahashi identity. The bare quantities are defined by using the field strength renormalization as

$$\psi_B = Z_{2t}^{1/2} \psi, \tag{2.23}$$

$$v_B = \frac{Z_{2s}}{Z_{2t}} v, \tag{2.24}$$

$$\varepsilon_B (A_0)_B^2 = Z_{3e} \varepsilon A_0^2, \tag{2.25}$$

$$\varepsilon_B \left( \frac{(A_\alpha)_B}{c_B} \right)^2 = Z_{3e} \varepsilon \left( \frac{A_\alpha}{c} \right)^2, \tag{2.26}$$

$$\frac{1}{\mu_B} \left( \frac{(A_\alpha)_B}{c_B} \right)^2 = Z_{3m} \frac{1}{\mu} \left( \frac{A_\alpha}{c} \right)^2, \tag{2.27}$$

$$c_B = \sqrt{\frac{Z_{3m}}{Z_{3e}}} c, \tag{2.28}$$

$$g_B = \frac{Z_{1t}}{Z_{2t} Z_{3e}^{1/2}} g = \frac{Z_{1s}}{Z_{2s} Z_{3e}^{1/2}} g = Z_{3e}^{-1/2} g. \tag{2.29}$$

These bare quantities must be independent of the renormalization scale  $\kappa_0$ . We use this fact to derive RG equations afterward.

### 2.2.3 The Ward–Takahashi Identity

We should confirm that the self-energy (2.8) and the vertex correction (2.13) and (2.14) satisfy the Ward–Takahashi identity [14, 15]. Here we consider the model without the Lorentz invariance, i.e.,  $v \neq c$ , we should be careful about the coefficients of the self-energy and the vertex correction.

The Ward–Takahashi identity is

$$-ik_\mu \Gamma^\mu(p+k, p) = G^{-1}(p+k) - G^{-1}(p), \quad (2.30)$$

where  $G(p)$  is the exact fermion propagator

$$G(p) = \frac{i}{\gamma^0 p_0 - v\boldsymbol{\gamma} \cdot \mathbf{p} - \Sigma(p)}, \quad (2.31)$$

and  $\Gamma^\mu(p+k, p)$  is the exact vertex. An important point here is that  $k_\mu$  in the left-hand side of Eq.(2.31) comes from the photon propagator, and hence  $k_\mu$  must be interpreted as

$$k^\mu = (k^0, ck^\alpha). \quad (2.32)$$

This formula holds even in this case without the Lorentz invariance.

From the Ward–Takahashi identity, we can find the relation between  $Z_1$  and  $Z_2$ . We separate the electron self-energy into the temporal and spatial parts as

$$\Sigma(p) = \Sigma^{(t)}\gamma^0 p_0 + \Sigma^{(s)}v\gamma^\alpha p_\alpha. \quad (2.33)$$

Then the Ward–Takahashi identity becomes

$$\begin{aligned} & -ik_0(\Gamma_0^0 + \delta\Gamma^0) - ick_\alpha(\Gamma_\alpha^\alpha + \delta\Gamma^\alpha) \\ &= -i(1 + \Sigma^{(t)})\gamma^0 k_0 - i(1 + \Sigma^{(s)})v\gamma^\alpha k_\alpha. \end{aligned} \quad (2.34)$$

Each quantity in parenthesis corresponds to  $Z_1$  or  $Z_2$ , except that the spatial component of the vertex correction includes a factor  $v/c$ . Therefore, we obtain

$$Z_{1t} = Z_{2t}, \quad (2.35)$$

$$Z_{2s} = Z_{2s}. \quad (2.36)$$

### 2.2.4 Power Counting

Before deriving RG equations, it is important to check the dimensions of several quantities. From the dimension of a quantity, we can easily presume the dependence of the quantity on the scale. We denote the physical dimensions of wavenumber  $[(\text{length})^{-1}]$  and frequency  $[(\text{time})^{-1}]$  as  $\Lambda$  and  $\Omega$ , respectively. We can determine the dimension of the Lagrangian since the action should be dimensionless, and thus

$$[\mathcal{L}] = [\Lambda^{d-1}\Omega^1]. \quad (2.37)$$

Then considering the Lagrangian (2.1), we obtain other relations as

$$[\psi] = [\Lambda^{(d-1)/2}], \quad (2.38)$$

$$[\varepsilon E^2] = [\Lambda^{d-1}\Omega^1], \quad (2.39)$$

$$[eE] = [\Lambda^1\Omega^1], \quad (2.40)$$

$$[g^2] = [\Lambda^{3-d}\Omega^1] = [(\text{velocity})^1\Lambda^\epsilon]. \quad (2.41)$$

The effective charge  $g$  is a marginal parameter in terms of the momentum dimension. To explicitly represent the engineering dimension of  $g^2$ , we substitute  $g^2$  with  $g^2\kappa^\epsilon$  in the original Lagrangian  $\mathcal{L}_0$  and the counterterm Lagrangian  $\mathcal{L}_{\text{c.t.}}$ . The bare values are momentum-scale invariant, and hence the bare value  $g_{\text{B}}$  does not change.

### 2.2.5 Derivation of Renormalization Group Equations

In this section, we derive the RG equations from the fact that bare values are independent of the momentum scale  $\kappa$ . The explicit forms for Eqs. (2.23), (2.28), and (2.29) are

$$v_{\text{B}} = v \left\{ 1 - \frac{2g^2}{3\pi\epsilon} \frac{c^2}{(c+v)^2v} \left[ 1 + 2\left(\frac{v}{c}\right) + \left(\frac{v}{c}\right)^2 - 4\left(\frac{v}{c}\right)^3 \right] \right\}, \quad (2.42)$$

$$c_{\text{B}} = c \left( 1 + \frac{Ng^2}{3\pi\epsilon} \frac{c^2 - v^2}{c^2v} \right), \quad (2.43)$$

$$g_{\text{B}}^2 = g^2\kappa^\epsilon \left( 1 + \frac{2Ng^2}{3\pi\epsilon} \frac{1}{v} \right). \quad (2.44)$$

Note that the physical values  $v$ ,  $c$ , and  $g$  are functions of the momentum scale  $\kappa$ . The bare quantities does not depend on  $\kappa$ , which leads to



$$\kappa \frac{dv_B}{d\kappa} = 0, \quad (2.45)$$

$$\kappa \frac{dc_B}{d\kappa} = 0, \quad (2.46)$$

$$\kappa \frac{dg_B^2}{d\kappa} = 0. \quad (2.47)$$

These equations can be written in a matrix form as

$$\left[ I + \frac{g^2}{\epsilon} A(\kappa) \right] \begin{pmatrix} \kappa \frac{dv}{d\kappa} \\ \kappa \frac{dc}{d\kappa} \\ \frac{1}{g^2} \kappa \frac{dg^2}{d\kappa} \end{pmatrix} = \begin{pmatrix} 0 \\ 0 \\ -\epsilon - g^2 b(\kappa) \end{pmatrix}, \quad (2.48)$$

where  $I = \text{diag}(1, 1, 1)$  and  $A = (a_{ij})$  are  $3 \times 3$  matrices, and  $a_{ij}(\kappa)$  and  $b(\kappa)$  are functions of  $v$  and  $c$ , which determine the perturbative corrections at order  $g^2$ . Now we consider the perturbative corrections to order  $g^2$  and take the limit  $\epsilon \rightarrow 0$  to obtain

$$\begin{aligned} \begin{pmatrix} \kappa \frac{dv}{d\kappa} \\ \kappa \frac{dc}{d\kappa} \\ \frac{1}{g^2} \kappa \frac{dg^2}{d\kappa} \end{pmatrix} &= \left[ I + \frac{g^2}{\epsilon} A \right]^{-1} \begin{pmatrix} 0 \\ 0 \\ -\epsilon - g^2 b \end{pmatrix} = \left[ I - \frac{g^2}{\epsilon} A \right] \begin{pmatrix} 0 \\ 0 \\ -\epsilon - g^2 b \end{pmatrix} + O(g^4) \\ &\xrightarrow{\epsilon \rightarrow 0} g^2 \begin{pmatrix} a_{13} \\ a_{23} \\ -b + a_{33} \end{pmatrix} + O(g^4). \end{aligned} \quad (2.49)$$

Finally, we obtain the RG equations

$$\kappa \frac{dv}{d\kappa} = -\frac{2g^2}{3\pi} \frac{c^2}{(c+v)^2} \left[ 1 + 2 \left( \frac{v}{c} \right) + \left( \frac{v}{c} \right)^2 - 4 \left( \frac{v}{c} \right)^3 \right], \quad (2.50)$$

$$\kappa \frac{dc}{d\kappa} = \frac{Ng^2}{3\pi} \frac{c^2 - v^2}{cv}, \quad (2.51)$$

$$\kappa \frac{dg^2}{d\kappa} = \frac{2Ng^4}{3\pi} \frac{1}{v}. \quad (2.52)$$

### 2.2.6 Numerical Solutions

The RG equations (2.50), (2.51), (2.52) cannot be solved analytically without any approximations, and thus we first solve them numerically. The numerical solutions

to the RG equations are shown in Figs. 2.2 and 2.3 for the initial (bare) values of  $v_0 = 0.001$  and  $\varepsilon_0 = 10$ . Here we consider a nonmagnetic material ( $\mu_0 = 1$ ). In this case,  $c_0 = 0.32$  and  $\alpha_0 = 0.73$ , where the dimensionless coupling constant  $\alpha$  is defined by

$$\alpha = \frac{g^2}{v} = \frac{e^2}{(4\pi\varepsilon)v}. \quad (2.53)$$

The numerical results show some important features. First, we can see that the quantity  $c^2 v^N$  is almost constant for all momentum scales and remains  $c_0^2 v_0^N$ . This fact helps the approximate but accurate analysis of the scaling functions as described below. Second, the speed of electron  $v$  and that of photon  $c$  approach to the common value  $c_\infty = (c_0^2 v_0^N)^{1/(N+2)}$  in the infrared limit. From the scale dependence of  $v$  and  $c$ , we can observe that there are three scaling regions and corresponding two crossovers,  $\kappa_1$  and  $\kappa_2$ .  $\kappa_1$  and  $\kappa_2$  are identified by the analytic solutions which we discuss below. Third, the coupling constant  $\alpha$  becomes small in the infrared region, which justifies our perturbative RG analysis. Therefore, quantum critical phenomena of 3D TIs and Weyl semimetals are ideal laboratories to study QED in solids, even though the Lorentz invariance is broken to a large extent in the original (bare) Lagrangian.

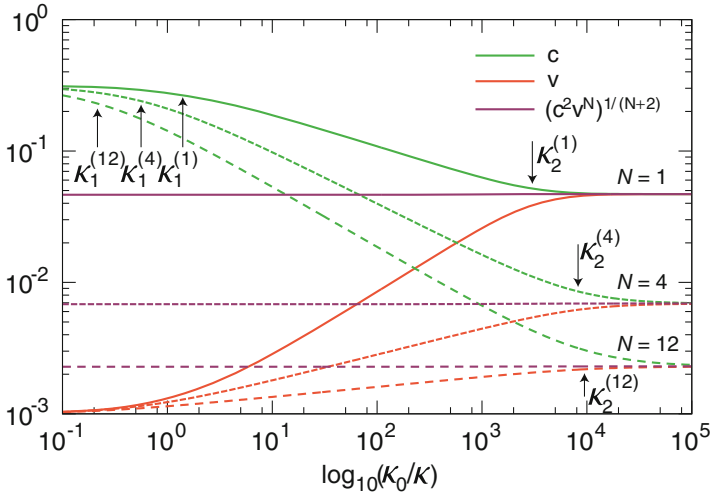


**Fig. 2.2** Numerical solutions to the RG equations for  $v$  and  $c$ . We set the initial values  $v_0 = 0.001$  and  $\varepsilon_0 = 10$ . A nonmagnetic material ( $\mu_0 = 1$ ) is considered, and in this case,  $c_0 = 0.32$  and  $\alpha_0 = 0.73$ . We can observe that the quantities  $(c^2 v^N)^{1/(N+2)}$  are almost constant for all momentum scale. Reprinted figure with permission from Ref. [13]. Copyright 2013 by the American Physical Society

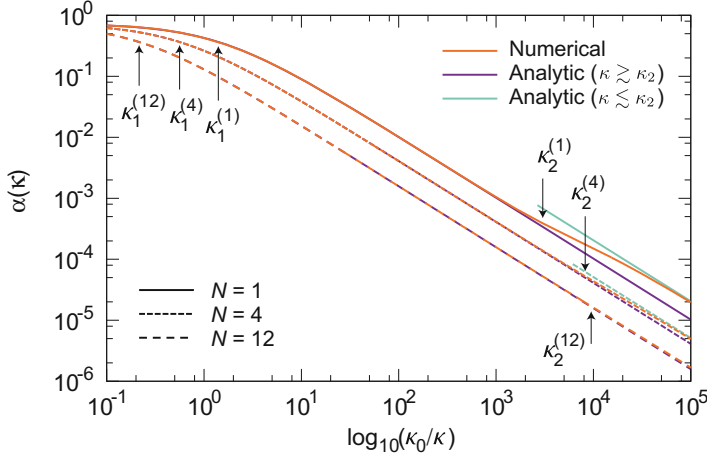


**Fig. 2.3** Numerical and analytic solutions to the RG equations for  $\alpha$ . The analytic solutions for  $\kappa \gtrsim \kappa_2$  and  $\kappa \lesssim \kappa_2$  well explain the numerical solutions. As the number of species  $N$  increases, the difference between the analytic and numerical solutions becomes smaller, and the analytic expression is more precise. Reprinted figure with permission from Ref. [13]. Copyright 2013 by the American Physical Society

### 2.2.7 Analytic Solutions

In this section, we investigate the analytic expressions for the RG equations. First, we define  $l = \ln(\kappa_0/\kappa)$  and consider the quantity  $c^2 v^N$ . From the RG equations, the scale dependence of this quantity is

$$\begin{aligned} \frac{d(c^2 v^N)}{dl} &= 2c v^N \frac{dc}{dl} + N c^2 v^{N-1} \frac{dv}{dl} \\ &= \frac{2N g^2}{3\pi} c^2 v^{N-1} \frac{\beta^2 (1 - \beta)^2}{(1 + \beta)^2}, \end{aligned} \quad (2.54)$$

with  $\beta = v/c$ . If we define the function  $f(\beta)$  as

$$f(\beta) = \frac{\beta^2 (1 - \beta)^2}{(1 + \beta)^2}, \quad (2.55)$$

and assume  $v \leq c$ , i.e.  $0 \leq \beta \leq 1$ , we obtain  $0 \leq g(x) \leq 17 - 12\sqrt{2} \simeq 0.03$ . The maximum value  $g(x) \simeq 0.03$  is rarely observed, and the right-hand side of Eq. (2.54) is always small for  $0 < \beta < 1$ . Therefore, the approximation

$$c^2 v^N = c_0^2 v_0^N \quad (2.56)$$

is satisfied for the entire energy scale.

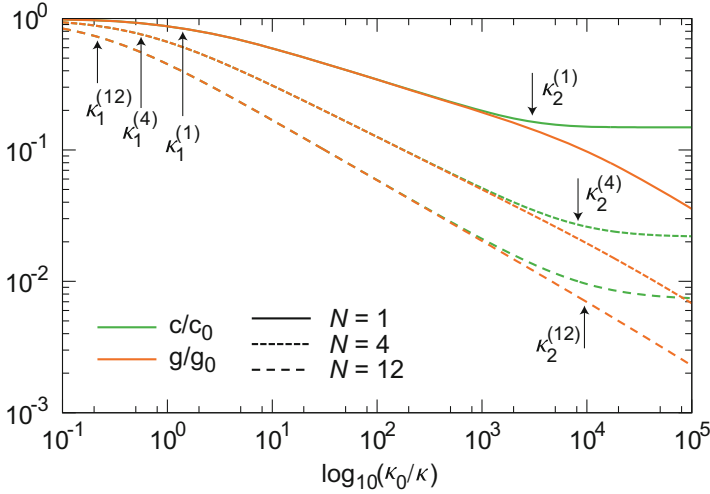


**Fig. 2.4** Numerical and analytic solutions to  $c$  and  $g$ . These two values coincide until  $c$  gets closer to the asymptotic value  $c_\infty$

The second approximation is

$$\frac{c}{c_0} = \frac{g}{g_0}, \quad (2.57)$$

which we can observe from the numerical calculation shown in Fig. 2.4, and it holds until  $c$  reaches the vicinity of the asymptotic value  $c_\infty$ . Actually, this approximation has a physical interpretation. Since  $c = 1/\sqrt{\varepsilon\mu}$  and  $g = e/\sqrt{4\pi\varepsilon}$ , the equality means the permeability  $\mu$  stays constant.

Using Eqs. (2.56) and (2.57), we can analytically solve the RG equations (2.50), (2.51), and (2.52), and we obtain

$$g^2(l) = g_0^2 \left( 1 + \frac{2N+2}{3\pi} \alpha_0 l \right)^{-N/(N+1)}. \quad (2.58)$$

The other solutions follow by using the analytic expression of  $g^2(l)$  as

$$v(l) = v_0 \left( 1 + \frac{2N+2}{3\pi} \alpha_0 l \right)^{1/(N+1)}, \quad (2.59)$$

$$c(l) = c_0 \left( 1 + \frac{2N+2}{3\pi} \alpha_0 l \right)^{-N/(2N+2)}, \quad (2.60)$$

$$\alpha(l) = \alpha_0 \left( 1 + \frac{2N+2}{3\pi} \alpha_0 l \right)^{-1}. \quad (2.61)$$

These analytic expressions are valid for  $\kappa \gtrsim \kappa_2$ .

From the analytical solutions, we can identify the two momentum scales,  $\kappa_1$  and  $\kappa_2$ , as

$$\kappa_1^{(N)} = \exp \left[ -\frac{3\pi}{(2N+2)\alpha_0} \right], \quad (2.62)$$

$$\kappa_2^{(N)} = \exp \left[ -\frac{3\pi}{(2N+2)\alpha_0} \left[ \left( \frac{c_0}{v_0} \right)^{(2N+2)/(N+2)} - 1 \right] \right]. \quad (2.63)$$

$\kappa_1$  is determined by  $\alpha(\kappa_1) = \alpha_0/2$  and  $\kappa_2$  is the point where the analytically-derived function  $c(\kappa)$  coincides with the asymptotic value  $c_\infty$ . Assuming  $v_0/c_0 \ll 1$ ,  $\kappa_2 \ll \kappa_1 < \kappa_0$  is satisfied. These two momenta separate the three regions: (i) perturbative region  $\kappa_1 \lesssim \kappa \lesssim \kappa_0$ , the renormalization effect is small and perturbative; (ii) nonrelativistic scaling region  $\kappa_2 \lesssim \kappa \lesssim \kappa_1$ , the renormalization effect is large, while  $c(\kappa) \gg v(\kappa)$  still holds; and (iii) relativistic scaling region  $\kappa \lesssim \kappa_2$ ,  $c(\kappa) \simeq v(\kappa)$  and the Lorentz invariance is recovered.

As to the dimensionless coupling constant  $\alpha$ , its analytic expression can be obtained for region (iii), the relativistic scaling region. When we put  $c = v = c_\infty$ , the RG equations for  $\alpha$  becomes

$$\frac{d\alpha}{dl} = -\frac{2N}{3\pi}\alpha^2, \quad (2.64)$$

and it can be solved analytically to obtain

$$\alpha(l) = \frac{3\pi}{2N} \frac{1}{l}. \quad (2.65)$$

Surprisingly, the coupling constant  $\alpha(l)$  in region (iii) is independent of its bare value  $\alpha_0$ . The approximate analytic solutions for  $\alpha$  [Eqs. (2.61) and (2.65)] are plotted in Fig. 2.3, together with the numerical solutions. The analytic solutions well agree with the numerical solutions, and we can observe the analytic solution (2.61) coincides with the numerical solution in the large- $N$  limit.

## 2.3 Density of States

The DOS is an important quantity to determine the physical property of a material. From the RG analysis, the electron velocity  $v(\kappa)$  is not a constant, and the energy  $E(k) = v(k)k$  is no longer linear in the momentum  $k$  below the cutoff. In general, the DOS of a system with energy  $E(k)$  is determined by

$$D(E) = \int \frac{d^3k}{(2\pi)^3} \delta(E - E(k)) = \frac{1}{2\pi^2} \frac{k^2(E)}{E'(k(E))}, \quad (2.66)$$

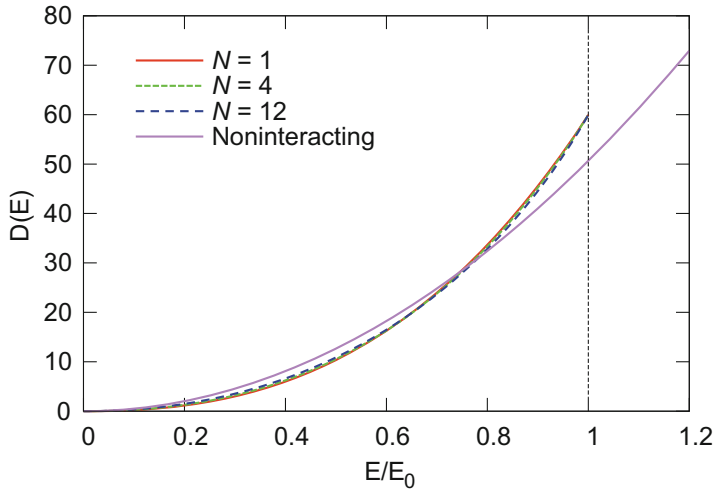


**Fig. 2.5** Density of states modified by the RG analysis. The DOS in the low-energy region is suppressed compared to the noninteracting one, due to the electron correlation effect. To compensate the suppression, the DOS increases around  $E/E_0 \gtrsim 0.8$ . The effect of RG appears only below the cutoff energy  $E_0$ . Reprinted figure with permission from Ref. [13]. Copyright 2013 by the American Physical Society

where  $E'$  stands for  $dE/dk$ . The DOS is a function of energy, and all quantities should be expressed in terms of energy  $E$ .

The DOS for 3D noninteracting Dirac fermions is

$$D_0(E) = \frac{E^2}{2\pi^2 v_0^3}. \quad (2.67)$$

The RG effect on the DOS is calculated numerically, and is compared with the noninteracting case in Fig. 2.5. Since  $v(\kappa)$  gets larger as the momentum scale goes to the infrared region, the DOS is suppressed in the low-energy region. On the other hand, the DOS is increased for  $0.8 \lesssim E/E_0 < 1$ , where  $E_0 = v_0 \kappa_0$  is the energy cutoff. This increase compensates the suppression of the DOS in the low-energy region.

## 2.4 Electromagnetic Properties

Let us discuss the permittivity  $\varepsilon(\kappa)$  and the permeability  $\mu(\kappa) = 1 + 4\pi\chi$  ( $\chi$ : magnetic susceptibility). The numerical solutions obtained from Eq.(2.52) and  $\mu = 1/(\varepsilon c^2)$  are shown in Fig. 2.6. We consider that the scale dependence of  $g^2$

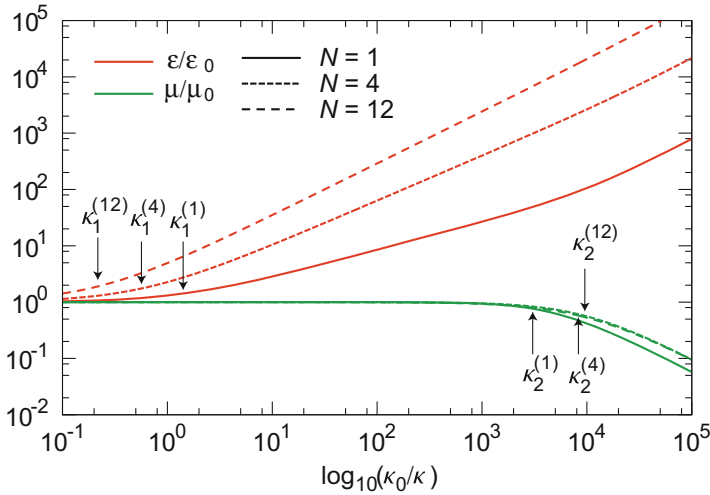


**Fig. 2.6** Numerical solutions to the RG equations for the permittivity  $\varepsilon$  and the permeability  $\mu$ . The characteristic momentum scales are different for  $\varepsilon$  and  $\mu$ . Reprinted figure with permission from Ref. [13]. Copyright 2013 by the American Physical Society

emerges only from  $\varepsilon$ , and that the bare electric charge  $e$  stays constant. For  $\kappa \gtrsim \kappa_2$ , the analytic solution to  $\varepsilon$  is easily obtained from Eq.(2.58) as

$$\varepsilon(l) = \varepsilon_0 \left( 1 + \frac{2N+2}{3\pi} \alpha_0 l \right)^{N/(N+1)}. \quad (2.68)$$

The momentum scale  $\kappa$  can be regarded as temperature  $T$  by  $T \simeq v(\kappa)\kappa$ . As noted above, the velocity  $v(\kappa)$  is the function of the momentum scale, hence the energy dispersion  $E(k) = v(k)k$  is a nonlinear function of  $k$ . From the definition of  $\kappa_1$  and  $\kappa_2$ ,  $v(\kappa_1) \simeq v_0$  and  $v(\kappa_2) \simeq c_\infty$ , and the corresponding temperatures are estimated as  $T_1 = T(\kappa_1) \simeq v_0\kappa_1$  and  $T_2 = T(\kappa_2) \simeq c_\infty\kappa_2$ . In Fig. 2.6, it can be seen that the permittivity  $\varepsilon(\kappa)$  grows logarithmically below  $T_1$  while the permeability  $\mu(\kappa)$  decreases below  $T_2$ . The orbital magnetic susceptibility  $\chi$  without electron-electron interaction logarithmically diverges as a function of  $T$ , but in our analysis, the logarithmic divergence is canceled due to the renormalization of  $v$ . These contrasting behaviors of  $\varepsilon$  and  $\mu$  facilitate the identification of  $T_1$  and  $T_2$  experimentally. In the zero temperature limit  $\varepsilon$  diverges while  $\mu$  goes to zero, i.e., the perfect diamagnetism  $\chi = -1/(4\pi)$  is accomplished.

## 2.5 Spectral Function

### 2.5.1 The Callan–Symanzik Equation

Before considering the spectral function, we discuss the scheme of the RG analysis. Here we handle the ultraviolet divergence by dimensional regularization, not by introducing the hard cutoff. In contrast to the Wilson’s picture of the renormalization, which includes the explicit cutoff scale, the dimensional regularization does not include a momentum scale in itself, and therefore, we introduced the *renormalization scale*  $\kappa_0$ . To define the theory at a different scale  $\kappa$ , we introduce the Callan–Symanzik equation [16–18].

Let  $G^{(n)}(\{p_i\}; v, c, \alpha; \kappa)$  be the connected  $n$ -point Green’s function, defined by

$$G^{(n)}(\{p_i\}; v, c, \alpha; \kappa) = \langle \Omega | \psi(p_1) \psi(p_2) \cdots \psi(p_n) | \Omega \rangle. \quad (2.69)$$

Here the running constants  $v$ ,  $c$ , and  $\alpha$  depend on the momentum scale  $\kappa$ . The renormalized Green’s function are equal to the bare Green’s function with a rescaling by the field strength renormalization  $Z_{2t}$ :

$$\langle \Omega | \psi_B(p_1) \psi_B(p_2) \cdots \psi_B(p_n) | \Omega \rangle = Z_{2t}^{n/2} \langle \Omega | \psi(p_1) \psi(p_2) \cdots \psi(p_n) | \Omega \rangle. \quad (2.70)$$

The left-hand side of Eq. (2.70) does not depend on the momentum scale  $\kappa$ . Differentiating Eq. (2.70) with respect to  $\kappa$  gives

$$0 = \left[ \kappa \frac{\partial}{\partial \kappa} + \kappa \frac{\partial v}{\partial \kappa} \frac{\partial}{\partial v} + \kappa \frac{\partial c}{\partial \kappa} \frac{\partial}{\partial c} + \kappa \frac{\partial \alpha}{\partial \kappa} \frac{\partial}{\partial \alpha} + \frac{n}{2} \kappa \frac{\partial \ln Z_{2t}}{\partial \kappa} \right] G^{(n)}. \quad (2.71)$$

Conventionally, the beta functions are defined in the following way:

$$\beta_v(\kappa) = \kappa \frac{\partial v}{\partial \kappa}, \quad (2.72)$$

$$\beta_c(\kappa) = \kappa \frac{\partial c}{\partial \kappa}, \quad (2.73)$$

$$\beta_\alpha(\kappa) = \kappa \frac{\partial \alpha}{\partial \kappa}. \quad (2.74)$$

We also define  $\gamma_2(\kappa)$ , which comes from the field renormalization, as

$$\gamma_2(\kappa) = \frac{1}{2} \kappa \frac{\partial \ln Z_{2t}}{\partial \kappa}. \quad (2.75)$$



Then, we obtain the Callan–Symanzik equation

$$\left[ \kappa \frac{\partial}{\partial \kappa} + \beta_v(\kappa) \frac{\partial}{\partial v} + \beta_c(\kappa) \frac{\partial}{\partial c} + \beta_\alpha(\kappa) \frac{\partial}{\partial \alpha} + n\gamma_2(\kappa) \right] G^{(n)}(\{p_i\}; v, c, \alpha; \kappa) = 0. \quad (2.76)$$

Since we already know that the dimension of the field operator is  $[\psi] = [\Lambda^{(d-1)/2}]$ , the engineering dimension of the Green's function is  $D = n(d-1)/2$ . Assuming that the Green's function is a homogeneous function in the momentum scale, we can confirm the relation

$$G^{(n)}(\{p_i, t\mathbf{p}_i\}; t^{-1}v, t^{-1}c, \alpha; t\kappa) = t^D G^{(n)}(\{p_i, \mathbf{p}_i\}; v, c, \alpha; \kappa). \quad (2.77)$$

Differentiating this equation by  $t$  and then setting  $t = 1$ , we obtain

$$\left[ \sum_i \mathbf{p}_i \cdot \frac{\partial}{\partial \mathbf{p}_i} - v \frac{\partial}{\partial v} - c \frac{\partial}{\partial c} + \kappa \frac{\partial}{\partial \kappa} \right] G^{(n)} = D G^{(n)}. \quad (2.78)$$

If the momentum  $\mathbf{p}_i$  is scaled with  $s$ , i.e.,  $\mathbf{p}_i$  is replaced by  $s\mathbf{p}_i$ , the derivative with respect to  $\mathbf{p}_i$  can be replaced as follows:

$$\sum_i \mathbf{p}_i \cdot \frac{\partial}{\partial \mathbf{p}_i} \rightarrow s \frac{\partial}{\partial s}. \quad (2.79)$$

Then, Eq. (2.78) becomes

$$\left[ s \frac{\partial}{\partial s} - v \frac{\partial}{\partial v} - c \frac{\partial}{\partial c} + \kappa \frac{\partial}{\partial \kappa} \right] G^{(n)} = D G^{(n)}. \quad (2.80)$$

From Eqs. (2.76) and (2.78), we can eliminate  $\kappa \partial / \partial \kappa$  and obtain

$$\left[ (\beta_v(\kappa) + v) \frac{\partial}{\partial v} + (\beta_c(\kappa) + c) \frac{\partial}{\partial c} + \beta_\alpha(\kappa) \frac{\partial}{\partial \alpha} + n\gamma_2(\kappa) - s \frac{\partial}{\partial s} \right] G^{(n)} = 0. \quad (2.81)$$

We need to solve this equation and investigate the dependence on  $s$ , which is equivalent to the momentum scale dependence.

The solution to the Callan–Symanzik equation is often obtained by using the bacteriological analogy introduced by Coleman [19]. We do not repeat the discussion here, but it is known in the conventional QED analysis that the solution to the Callan–Symanzik equation is obtained by replacing the original (constant) parameters to the running parameters, and multiplying the contribution from  $\gamma_2$ , originated from the field strength renormalization. For a two-point Green's function, i.e., a usual electron Green's function  $G(\mathbf{k}, \omega)$ , it is modified according to the Callan–Symanzik equation as

$$G(\mathbf{k}, \omega) = \frac{\mathcal{G}(\alpha(\kappa))}{\omega^2 - v^2(\kappa)\mathbf{k}^2} \exp \left[ 2 \int_{\Lambda}^k d \ln \left( \frac{k'}{\Lambda} \right) \gamma_2(\alpha) \right], \quad (2.82)$$

where  $\Lambda$  is the energy cutoff, and  $\mathcal{G}$  is a function determined from a perturbative renormalization calculation.  $k$  in this equation is a spacelike momentum, and should be considered as  $k = \sqrt{v^2 \mathbf{k}^2 - \omega^2}$ .

### 2.5.2 Spectral Function

To derive the spectral function as the imaginary part of the Green's function, we should be careful on the choice of the gauge, because the Green's function itself depends on the gauge. We adopt the “physical gauge,” i.e., Coulomb gauge. In Coulomb gauge, the photon propagator  $D_C^{\mu\nu}(k)$  is given by [20]

$$D_C^{\mu\nu}(k) = \frac{c^2}{\epsilon} \begin{pmatrix} \frac{1}{\mathbf{k}^2} & 0 \\ 0 & -\frac{g^{\alpha\beta}}{k^2} - \frac{1}{k^2} \frac{k^\alpha k^\beta}{\mathbf{k}^2} \end{pmatrix}. \quad (2.83)$$

We need to calculate the one-loop self-energy (Fig. 2.1a) by using the photon propagator in Coulomb gauge. The electron propagator is the same as before. After some calculation, we obtain the one-loop self-energy in Coulomb gauge  $\Sigma_2^{(C)}(p)$  as

$$\begin{aligned} \Sigma_2^{(C)}(p) = & -\frac{2g^2}{\pi} \frac{v^2}{c(c+v)^2} \left( \frac{1}{\epsilon} - \frac{1}{2} \ln \frac{e^\gamma}{4\pi} \right) \gamma^0 p_0 \\ & + \frac{2g^2}{3\pi} \frac{c^2}{v(c+v)^2} \left[ 1 + 2 \left( \frac{v}{c} \right) + \left( \frac{v}{c} \right)^2 - \left( \frac{v}{c} \right)^3 \right] \left( \frac{1}{\epsilon} - \frac{1}{2} \ln \frac{e^\gamma}{4\pi} \right) v \boldsymbol{\gamma} \cdot \mathbf{p}, \end{aligned} \quad (2.84)$$

where  $\gamma \approx 0.57721$  is the Euler–Mascheroni constant. For a later use, we show the result to order  $O(\epsilon^0)$ . The self-energy in Coulomb gauge [Eq. (2.84)] is different from the self-energy in Feynman gauge [Eq. (2.8)], comparing the  $O(\epsilon^{-1})$  contributions.

The field strength renormalization  $Z_{2t}^{(C)}$  and  $Z_{2s}^{(C)}$  in Coulomb gauge are

$$Z_{2t}^{(C)} = 1 - \frac{2g^2}{\pi\epsilon} \frac{v^2}{c(c+v)^2}, \quad (2.85)$$

$$Z_{2s}^{(C)} = 1 - \frac{2g^2}{3\pi\epsilon} \frac{c^2}{v(c+v)^2} \left[ 1 + 2 \left( \frac{v}{c} \right) + \left( \frac{v}{c} \right)^2 - \left( \frac{v}{c} \right)^3 \right]. \quad (2.86)$$

This difference alters the Green's function and also the spectral function, while the physical quantities, e.g., the electron velocity  $v$ , remain the same.<sup>2</sup> For the spectral function of electrons, the function  $\gamma_2(\kappa)$  in Coulomb gauge is required, which is given by

$$\gamma_2^{(C)}(v, c, \alpha; \kappa) = \frac{1}{2} \kappa \frac{d \ln Z_{2t}^{(C)}}{d\kappa} = \frac{g^2}{\pi} \frac{v^2}{c(c+v)^2}. \quad (2.87)$$

In principle, ARPES can measure the energy dispersion  $E(k) = v(\kappa)|\mathbf{k}|$ , which shows crossovers at  $\kappa_1$  and  $\kappa_2$ . From the Callan–Symanzik equation, the electron Green's function in Coulomb gauge  $G^{(C)}(\mathbf{k}, \omega)$  is

$$G^{(C)}(\mathbf{k}, \omega) = \frac{\mathcal{G}(\alpha(\kappa))}{\omega^2 - v^2(\kappa)\mathbf{k}^2} \exp \left[ 2 \int_{\Lambda}^k d \ln \left( \frac{k'}{\Lambda} \right) \gamma_2^{(C)}(\alpha) \right]. \quad (2.88)$$

In region (i),  $\gamma_2^{(C)} = 0$ , and the Green's function is unchanged. In region (ii),  $\kappa$  dependence of  $\gamma_2^{(C)}$  is rather complicated to calculate  $G(\mathbf{k}, \omega)$ , and thus we only consider the relativistic scaling region (iii), where  $v$  approaches  $c$  and the original QED regime is applicable. By using the analytic solution to  $\alpha$  [Eq.(2.65)],  $\gamma_2^{(C)}(k)$  is expressed as

$$\gamma_2^{(C)}(k) = \frac{\alpha(k)}{4\pi} = \frac{3}{8N} \left[ \ln \left( \frac{\Lambda}{k} \right) \right]^{-1}. \quad (2.89)$$

The perturbative correction  $\mathcal{G}$  is obtained from the  $O(\epsilon^0)$  contribution of  $\Sigma_2^{(C)}(p)$  [see Eq.(2.84)], since the divergent part, which is proportional to  $1/\epsilon$ , is eliminated by the counterterms. Therefore, the perturbative correction  $\mathcal{G}$  is

$$\mathcal{G}(\alpha(k)) = 1 + \frac{\alpha(k)}{4\pi} \ln \left( \frac{e^\gamma}{4\pi} \right) + O(\alpha^2). \quad (2.90)$$

Finally, we obtain the electron Green's function

$$G(\mathbf{k}, \omega) = \frac{\mathcal{G}(\alpha(k))}{\omega^2 - c_\infty^2 \mathbf{k}^2} \left[ \frac{1}{2} \ln \left( \frac{\Lambda^2}{c_\infty^2 \mathbf{k}^2 - \omega^2} \right) \right]^{-3/(4N)}. \quad (2.91)$$

By substituting  $\omega$  with  $\omega + i0$ , the imaginary part of the Green's function  $-\text{Im}G(\mathbf{k}, \omega)$  gives the electron spectral function. The electron spectral function has finite values for  $|\omega| \geq c_\infty|\mathbf{k}|$ , otherwise  $-\text{Im}G(\mathbf{k}, \omega) = 0$ . As depicted in Fig.2.7,

---

<sup>2</sup>For example, we calculate the electron velocity  $v$  in Coulomb gauge. Its bare value is obtained by

$$v_B = v \frac{Z_{2s}^{(C)}}{Z_{2t}^{(C)}} = v \left\{ 1 - \frac{2g^2}{3\pi\epsilon} \frac{c^2}{v(c+v)^2} \left[ 1 + 2 \left( \frac{v}{c} \right) + \left( \frac{v}{c} \right)^2 - 4 \left( \frac{v}{c} \right)^3 \right] \right\}.$$

We can see that this equation is exactly the same as the previous result in Feynman gauge [Eq.(2.42)]. Thus, the running electron velocity  $v(\kappa)$  is unchanged whichever gauge we choose.

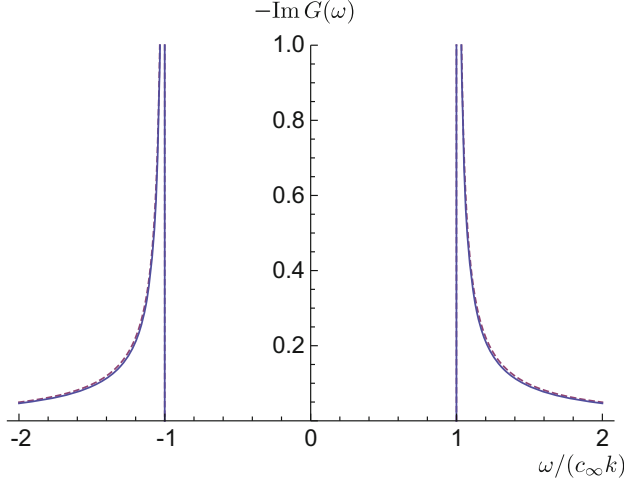


**Fig. 2.7** Frequency dependence of the spectral function in region (iii) with  $N = 1$ . The *solid line* denotes the result with the perturbative correction in  $\mathcal{G}$ , while the *dashed line* depicts the result for  $\mathcal{G} = 1$

the perturbative correction for  $\mathcal{G}$  gives very small contribution, and hence we put  $\mathcal{G} = 1$  in the following analysis. Then, the spectral function in region (iii) has the approximate form

$$\begin{aligned}
 & -\text{Im}G(\mathbf{k}, \omega) \\
 & \sim a\delta(\omega^2 - c_\infty^2 \mathbf{k}^2) + \frac{1}{\omega^2 - c_\infty^2 \mathbf{k}^2} \frac{3\pi}{8N} \left[ \frac{1}{2} \ln \left| \frac{\Lambda^2}{c_\infty^2 \mathbf{k}^2 - \omega^2} \right| \right]^{-1-3/(4N)} \theta(\omega^2 - c_\infty^2 \mathbf{k}^2),
 \end{aligned} \tag{2.92}$$

where the residue  $a$  is a constant determined from the sum rule. The  $\delta$  function peak with finite  $a$  means that the system remains a Fermi liquid in sharp contrast to the (2+1)D case [5], while the continuum state for  $|\omega| > c_\infty k$  comes from the interaction effect.

## 2.6 Electric Conductivity

In this section, we derive the conductivity of the system with  $N_W$  Weyl nodes by solving the quantum Boltzmann equation (QBE). The RG analysis above is performed for the massless Dirac fermions with  $N$  species. One massless Dirac fermion can be separated into two Weyl fermions with opposite chiralities, and therefore,  $N$  Dirac nodes can be interpreted as  $2N$  Weyl nodes, i.e.,  $N_W = 2N$ .

### 2.6.1 The Quantum Boltzmann Equation

The QBE is the matrix equation, whose elements are labeled by fermion species, spin, and helicity indices. We focus on the right-handed electron with species  $a$ , and there are  $N$  copies of right-handed electrons and a corresponding number of left-handed particles.

Calculations are done by following previous studies [7, 21, 22]. We only focus on the diagonal elements of the QBE, which describe the distribution functions of particles and holes  $f_{\lambda a}(\mathbf{k}, t)$ . Here,  $\lambda = \pm$  represents a particle ( $\lambda = +$ ) or a hole ( $\lambda = -$ ), and  $a$  denotes a Weyl fermion species. The off-diagonal elements correspond to the particle-hole pair contribution, and for  $\omega \ll T$ , its contribution is suppressed [7]. Then, the QBE in the external field  $\mathbf{F}$  is

$$\left[ \frac{\partial}{\partial t} + \mathbf{F} \cdot \frac{\partial}{\partial \mathbf{k}} \right] f_{\lambda a}(\mathbf{k}, t) = -w[f_{\lambda a}(\mathbf{k}, t)], \quad (2.93)$$

where the scattering rate  $w$  reflects the electron correlation effect. The scattering rate  $w[f_{\lambda a}(\mathbf{k}, t)]$  is written as

$$\begin{aligned} w[f_{\lambda a}(\mathbf{k}, t)] = & \frac{1}{2} \sum_{\substack{bcd \\ \lambda_1 \lambda_2 \lambda_3}} \int_{\mathbf{p}, \mathbf{k}', \mathbf{p}'} \left| M_{\lambda_2 c, \lambda_3 d}^{\lambda a, \lambda_1 b}(k, p, k', p') \right|^2 \\ & \times (2\pi) \delta(E_{\lambda a}(k) + E_{\lambda_1 b}(p) - E_{\lambda_2 c}(k') - E_{\lambda_3 d}(p')) \\ & \times (2\pi)^3 \delta^{(3)}(\mathbf{k} + \mathbf{p} - \mathbf{k}' - \mathbf{p}') \\ & \times \{ f_{\lambda a}(\mathbf{k}, t) f_{\lambda_1 b}(\mathbf{p}, t) [1 - f_{\lambda_2 c}(\mathbf{k}', t)] [1 - f_{\lambda_3 d}(\mathbf{p}', t)] \\ & - [1 - f_{\lambda a}(\mathbf{k}, t)] [1 - f_{\lambda_1 b}(\mathbf{p}, t)] f_{\lambda_2 c}(\mathbf{k}', t) f_{\lambda_3 d}(\mathbf{p}', t) \}. \end{aligned} \quad (2.94)$$

In this section, we use the convention  $\int_{\mathbf{p}} = \int \frac{d^3 p}{(2\pi)^3}$ . Here,  $E_{\lambda a}(k) = \lambda v k$  is the energy of the  $a$ -th Weyl node. We only consider the two-body scattering, and  $M_{\lambda_2 c, \lambda_3 d}^{\lambda a, \lambda_1 b}(k, p, k', p')$  is the scattering amplitude with nonrelativistic renormalization (Fig. 2.8). The relation to the relativistic scattering amplitude  $\mathcal{M}$  is

$$\left| M_{\lambda_2 c, \lambda_3 d}^{\lambda a, \lambda_1 b}(k, p, k', p') \right|^2 = \frac{\left| \mathcal{M}_{\lambda_2 c, \lambda_3 d}^{\lambda a, \lambda_1 b}(k, p, k', p') \right|^2}{(2E_{\lambda a})(2E_{\lambda_1 b})(2E_{\lambda_2 c})(2E_{\lambda_3 d})}. \quad (2.95)$$

We assume that the external electric force  $\mathbf{F} = e\mathbf{E}$  is weak, and that the deviation of the distribution function from the equilibrium  $f_{\lambda a}^0(k) = (1 + e^{\beta E_{\lambda a}(k)})^{-1}$  is small, so that we consider the linear response in  $\mathbf{E}$ :

$$f_{\lambda a}(\mathbf{k}, \omega) = 2\pi \delta(\omega) f_{\lambda a}^0(k) + \lambda \frac{\mathbf{k} \cdot e\mathbf{E}(\omega)}{k} f_{\lambda a}^0(k) [1 - f_{\lambda a}^0(k)] g_a(k, \omega). \quad (2.96)$$

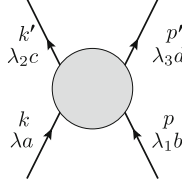


**Fig. 2.8** Diagrammatic representation of two-body scatterings. Its nonrelativistic scattering amplitude is given by  $M_{\lambda_2c, \lambda_3d}^{\lambda a, \lambda_1b}(k, p, k', p')$ . The gray circle corresponds to various scattering processes

The current density  $\mathbf{j}(\omega)$  without the particle-hole pair contribution is

$$\mathbf{j}(\omega) = ev \sum_{\lambda a} \int_{\mathbf{k}} \frac{\lambda \mathbf{k}}{k} f_{\lambda a}(\mathbf{k}, \omega), \quad (2.97)$$

and therefore, the electric conductivity  $\sigma(\omega)$  is given by using the function  $g_a(k, \omega)$  as

$$\sigma(\omega) = \frac{j(\omega)}{E(\omega)} = e^2 v \sum_{\lambda a} \int_{\mathbf{k}} \frac{k_x^2}{k^2} f_{\lambda a}^0(k) [1 - f_{\lambda a}^0(k)] g_a(k, \omega). \quad (2.98)$$

We should determine  $g_a(k, \omega)$  to obtain the electric conductivity. In equilibrium, the scattering rate vanishes, i.e.,  $w[f^0] = 0$ , and thus when we expand the scattering rate in terms of  $g_a(k, \omega)$ , the zeroth order term vanishes. Therefore, we can write

$$w[f_{\lambda a}(\mathbf{k}, \omega)] = e \mathbf{E}(\omega) \cdot \mathcal{C}[\lambda \hat{\mathbf{k}} g_a(k, \omega)] + O(g^2), \quad (2.99)$$

where  $\hat{\mathbf{k}} = \mathbf{k}/k$ , and  $\mathcal{C}$  is called the collision operator. The collision operator is given by

$$\begin{aligned} & \mathcal{C}[\lambda \hat{\mathbf{k}} g_a(k, \omega)] \\ &= \frac{1}{2} \sum_{\substack{bcd \\ \lambda_1 \lambda_2 \lambda_3}} \int_{\mathbf{p}, \mathbf{k}', \mathbf{p}'} \left| M_{\lambda_2c, \lambda_3d}^{\lambda a, \lambda_1b}(k, p, k', p') \right|^2 \\ & \quad \times (2\pi) \delta(E_{\lambda a}(k) + E_{\lambda_1b}(p) - E_{\lambda_2c}(k') - E_{\lambda_3d}(p')) \\ & \quad \times (2\pi)^3 \delta^{(3)}(\mathbf{k} + \mathbf{p} - \mathbf{k}' - \mathbf{p}') \\ & \quad \times f_{\lambda a}^0(k) f_{\lambda_1b}^0(p) [1 - f_{\lambda_2c}^0(k')] [1 - f_{\lambda_3d}^0(p')] \\ & \quad \times \left[ \lambda \hat{\mathbf{k}} g_a(k, \omega) + \lambda_1 \hat{\mathbf{p}} g_b(p, \omega) - \lambda_2 \hat{\mathbf{k}}' g_c(k', \omega) - \lambda_3 \hat{\mathbf{p}}' g_d(p', \omega) \right]. \end{aligned} \quad (2.100)$$

By using the collision operator, the QBE becomes

$$[i\omega g_a(k, \omega) + \beta v] \lambda \hat{\mathbf{k}} f_{\lambda a}^0(k) [1 - f_{\lambda a}^0(k)] = \mathcal{C}[\lambda \hat{\mathbf{k}} g_a(k, \omega)]. \quad (2.101)$$

To solve this equation, it is convenient to use a variational method. The variational functional  $\mathcal{Q}[g]$  is derived by defining the inner product. We define the inner product as

$$\langle F, G \rangle = \sum_a \int_{\mathbf{k}} F_a(\mathbf{k}) \cdot G_a(\mathbf{k}), \quad (2.102)$$

and the functional  $\mathcal{Q}[g]$  is given by

$$\begin{aligned} \mathcal{Q}[g] &= \sum_a \int_{\mathbf{k}} \left[ i\omega \frac{g_a^2(k, \omega)}{2} + \beta v g_a(k, \omega) \right] f_{\lambda a}^0(k) [1 - f_{\lambda a}^0(k)] - \frac{1}{2} \langle \lambda \hat{\mathbf{k}} g_a(k, \omega), \mathcal{C}[\lambda \hat{\mathbf{k}} g_a(k, \omega)] \rangle. \end{aligned} \quad (2.103)$$

The product  $\langle \lambda \hat{\mathbf{k}} g_a, \mathcal{C}[\lambda \hat{\mathbf{k}} g_a] \rangle$  is expressed as

$$\begin{aligned} &\langle \lambda \hat{\mathbf{k}} g_a, \mathcal{C}[\lambda \hat{\mathbf{k}} g_a] \rangle \\ &= \frac{1}{8} \sum_{\substack{abcd \\ \lambda_1 \lambda_2 \lambda_3}} \int_{\mathbf{k}, \mathbf{p}, \mathbf{q}} \left| M_{\lambda_2 c, \lambda_3 d}^{\lambda a, \lambda_1 b} \right|^2 (2\pi) \delta(E_{\lambda a}(k) + E_{\lambda_1 b}(p) - E_{\lambda_2 c}(k') - E_{\lambda_3 d}(p')) \\ &\quad \times f_{\lambda a}^0(k) f_{\lambda_1 b}^0(p) [1 - f_{\lambda_2 c}^0(|\mathbf{k} + \mathbf{q}|)] [1 - f_{\lambda_3 d}^0(|\mathbf{p} - \mathbf{q}|)] \\ &\quad \times \left[ \lambda \frac{\mathbf{k}}{|\mathbf{k}|} g_a(k, \omega) + \lambda_1 \frac{\mathbf{p}}{|\mathbf{p}|} g_b(p, \omega) \right. \\ &\quad \left. - \lambda_2 \frac{\mathbf{k} + \mathbf{q}}{|\mathbf{k} + \mathbf{q}|} g_c(|\mathbf{k} + \mathbf{q}|, \omega) - \lambda_3 \frac{\mathbf{p} - \mathbf{q}}{|\mathbf{p} - \mathbf{q}|} g_d(|\mathbf{p} - \mathbf{q}|, \omega) \right]^2, \end{aligned} \quad (2.104)$$

where  $\mathbf{q} = \mathbf{k}' - \mathbf{k}$  comes from the momentum conservation. In this calculation, we assume that all Weyl nodes are equivalent, i.e.,  $f_{\lambda a}^0(k)$  and  $g_a(k, \omega)$  is independent of the species. Thus, we omit the index  $a$  and use  $f_{\lambda}^0(k)$  and  $g(k, \omega)$  in the following calculation. The stationary point

$$\frac{\delta \mathcal{Q}[g]}{\delta g} = 0 \quad (2.105)$$

gives the solution to  $g(k, \omega)$ .

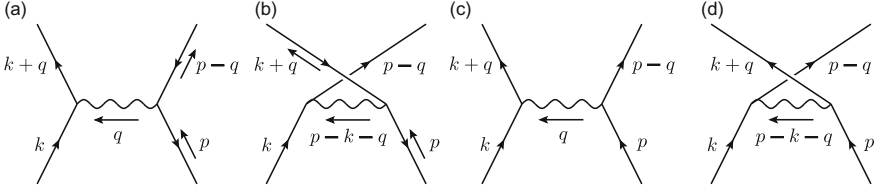


**Fig. 2.9** Feynman diagrams for the leading order two-particle scattering processes. **a** and **b** represent electron-hole scatterings, and **c** and **d** electron-electron scatterings. The  $t$ -channel diagrams **a**, **c** contribute to the leading order, and the  $u$ -channel diagrams **b**, **d** do not

### 2.6.2 Scattering Rate

The next task is to calculate the functional  $\langle \lambda \hat{\mathbf{k}} g_a, \mathcal{C}[\lambda \hat{\mathbf{k}} g_a] \rangle$ . For simplicity, we set  $\lambda = +$  and  $a = R$ , where the handedness of the species is represented as  $a = R$  or  $L$ . We consider two-body scatterings to the leading order, and then there are four scattering processes (Fig. 2.9). We write the scattering rates of electron-hole and electron-electron processes as  $R_1(\mathbf{k}, \mathbf{p}, \mathbf{q})$  and  $R_2(\mathbf{k}, \mathbf{p}, \mathbf{q})$ , respectively, where  $\mathbf{k}$  and  $\mathbf{p}$  are the momenta of the incoming particles and  $\mathbf{q}$  is the momentum of the virtual photon. Similarly, we denote the scattering amplitude  $M_{\lambda_2 c, \lambda_3 d}^{\lambda a, \lambda_1 b}(\mathbf{k}, \mathbf{p}, \mathbf{k}', \mathbf{p}') = M_{\lambda_2 c, \lambda_3 d}^{\lambda a, \lambda_1 b}(\mathbf{k}, \mathbf{p}, \mathbf{k}' - \mathbf{k})$  for the convenience of later analysis. Then, the functional  $\langle \hat{\mathbf{k}} g, \mathcal{C}[\hat{\mathbf{k}} g] \rangle$  becomes

$$\begin{aligned}
 & \langle \hat{\mathbf{k}} g, \mathcal{C}[\hat{\mathbf{k}} g] \rangle \\
 &= \frac{1}{8} \int_{\mathbf{k}, \mathbf{p}, \mathbf{q}} \frac{2\pi}{v} \left\{ \delta(k - p - |\mathbf{k} + \mathbf{q}| + |\mathbf{p} - \mathbf{q}|) \right. \\
 & \quad \times f_+^0(k) f_-^0(p) [1 - f_+^0(|\mathbf{k} + \mathbf{q}|)] [1 - f_-^0(|\mathbf{p} - \mathbf{q}|)] R_1(\mathbf{k}, \mathbf{p}, \mathbf{q}) \\
 & \quad \times \left[ \frac{\mathbf{k}}{|\mathbf{k}|} g(k, \omega) - \frac{\mathbf{p}}{|\mathbf{p}|} g(p, \omega) - \frac{\mathbf{k} + \mathbf{q}}{|\mathbf{k} + \mathbf{q}|} g(|\mathbf{k} + \mathbf{q}|, \omega) + \frac{\mathbf{p} - \mathbf{q}}{|\mathbf{p} - \mathbf{q}|} g(|\mathbf{p} - \mathbf{q}|, \omega) \right]^2 \\
 & \quad + \delta(k + p - |\mathbf{k} + \mathbf{q}| - |\mathbf{p} - \mathbf{q}|) \\
 & \quad \times f_+^0(k) f_+^0(p) [1 - f_+^0(|\mathbf{k} + \mathbf{q}|)] [1 - f_+^0(|\mathbf{p} - \mathbf{q}|)] R_2(\mathbf{k}, \mathbf{p}, \mathbf{q}) \\
 & \quad \times \left[ \frac{\mathbf{k}}{|\mathbf{k}|} g(k, \omega) + \frac{\mathbf{p}}{|\mathbf{p}|} g(p, \omega) - \frac{\mathbf{k} + \mathbf{q}}{|\mathbf{k} + \mathbf{q}|} g(|\mathbf{k} + \mathbf{q}|, \omega) - \frac{\mathbf{p} - \mathbf{q}}{|\mathbf{p} - \mathbf{q}|} g(|\mathbf{p} - \mathbf{q}|, \omega) \right]^2 \left. \right\}, \tag{2.106}
 \end{aligned}$$

and the scattering rate is

$$\begin{aligned}
 R_1(\mathbf{k}, \mathbf{p}, \mathbf{q}) &= |M_{+R, -R}^{+R, -R}(\mathbf{k}, \mathbf{p}, \mathbf{q}) - M_{-R, +R}^{+R, -R}(\mathbf{k}, \mathbf{p}, \mathbf{p} - \mathbf{k} - \mathbf{q})|^2 \\
 & \quad + (N - 1) \left[ |M_{+R, -R}^{+R, -R}(\mathbf{k}, \mathbf{p}, \mathbf{q})|^2 + |M_{-R, +R}^{+R, -R}(\mathbf{k}, \mathbf{p}, \mathbf{p} - \mathbf{k} - \mathbf{q})|^2 \right] \\
 & \quad + N \left[ |M_{+R, -L}^{+R, -L}(\mathbf{k}, \mathbf{p}, \mathbf{q})|^2 + |M_{-L, +R}^{+R, -L}(\mathbf{k}, \mathbf{p}, \mathbf{p} - \mathbf{k} - \mathbf{q})|^2 \right]
 \end{aligned}$$



$$R_2(\mathbf{k}, \mathbf{p}, \mathbf{q}) = \frac{1}{2} |M_{+R,+R}^{+R,+R}(\mathbf{k}, \mathbf{p}, \mathbf{q}) - M_{+R,+R}^{+R,+R}(\mathbf{k}, \mathbf{p}, \mathbf{p} - \mathbf{k} - \mathbf{q})|^2 \\ + (N - 1) |M_{+R,+R}^{+R,+R}(\mathbf{k}, \mathbf{p}, \mathbf{q})|^2 + N |M_{+R,+L}^{+R,+L}(\mathbf{k}, \mathbf{p}, \mathbf{q})|^2. \quad (2.107)$$

We assume the form  $g(k, \omega) = k\xi(\omega)$  according to Refs. [7, 22]. In this case, only the electron-hole scatterings  $R_1$  (Fig. 2.9a, b) contribute, while the electron-electron scatterings  $R_2$  (Fig. 2.9c, d) do not.

In the leading log approximation (LLA), the divergence at small  $q$  plays a key role. In other words, the integrand proportional to  $1/q$  gives a logarithmic divergence, and this is the dominant contribution in the LLA. The photon propagator in the  $t$ -channel diagrams (Fig. 2.9a, c) gives  $1/q^2$  contribution as we can see from the Feynman diagrams. Then, the integrand is proportional to  $1/q$ , and hence the contribution from the  $t$ -channel diagrams must be retained. On the other hand, the  $u$ -channel diagrams (Fig. 2.9b, d) give finite contributions, and they can be ignored in the LLA.

Therefore, it is necessary to calculate the  $t$ -channel diagrams of the electron-hole scatterings, i.e.,

$$R_1(\mathbf{k}, \mathbf{p}, \mathbf{q}) \sim N |M_{+R,-R}^{+R,-R}(\mathbf{k}, \mathbf{p}, \mathbf{q})|^2 + N |M_{+R,-L}^{+R,-L}(\mathbf{k}, \mathbf{p}, \mathbf{q})|^2. \quad (2.108)$$

For a later use, we write the delta function originated from the energy conservation as

$$\delta(k - p - |\mathbf{k} + \mathbf{q}| + |\mathbf{p} - \mathbf{q}|) = \int_{-\infty}^{\infty} \delta(k - |\mathbf{k} + \mathbf{q}| + \Omega) \delta(p - |\mathbf{p} - \mathbf{q}| + \Omega) d\Omega. \quad (2.109)$$

By using the projection operators  $(1 \pm \gamma^5)/2$ , we can calculate the relativistic scattering rates  $|\mathcal{M}_{+R,-R}^{+R,-R}(k, p, k', p')|^2$  and  $|\mathcal{M}_{+R,-L}^{+R,-L}(k, p, k', p')|^2$ . After some calculations and taking spin sums, the scattering rates become

$$\sum_{\text{spins}} |\mathcal{M}_{+R,-R}^{+R,-R}(k, p, k', p')|^2 \\ = \frac{8e^4 c^4}{\varepsilon q_p^4} \left\{ (l_{\mathbf{k}_e} \cdot l_{\mathbf{p}_e})(l_{\mathbf{k}'_e} \cdot l_{\mathbf{p}'_e}) + (l_{\mathbf{k}_e} \cdot l_{\mathbf{p}'_e})(l_{\mathbf{k}'_e} \cdot l_{\mathbf{p}_e}) \right. \\ \left. - (l^2_{\mathbf{k}_e} \cdot l^2_{\mathbf{k}'_e})(p_e \cdot p'_e) - (k_e \cdot k'_e)(l^2_{\mathbf{p}_e} \cdot l^2_{\mathbf{p}'_e}) \right. \\ \left. + \frac{1}{2} \left[ 1 + 3 \left( \frac{v}{c} \right) \right] (k_e \cdot k'_e)(p_e \cdot p'_e) + \left( \frac{v}{c} \right)^6 \left[ (k_p \cdot p'_p)(k'_p \cdot p_e) - (k_p \cdot p_p)(k'_p \cdot p'_p) \right] \right\}, \quad (2.110)$$

$$\sum_{\text{spins}} |\mathcal{M}_{+R,-L}^{+R,-L}(k, p, k', p')|^2 \\ = \frac{8e^4 c^4}{\varepsilon q_p^4} \left\{ (l_{\mathbf{k}_e} \cdot l_{\mathbf{p}_e})(l_{\mathbf{k}'_e} \cdot l_{\mathbf{p}'_e}) + (l_{\mathbf{k}_e} \cdot l_{\mathbf{p}'_e})(l_{\mathbf{k}'_e} \cdot l_{\mathbf{p}_e}) \right.$$

$$\begin{aligned}
& - (l^2 k_e \cdot l^2 k'_e)(p_e \cdot p'_e) - (k_e \cdot k'_e)(l^2 p_e \cdot l^2 p'_e) \\
& + \frac{1}{2} \left[ 1 + 3 \left( \frac{v}{c} \right) \right] (k_e \cdot k'_e)(p_e \cdot p'_e) - \left( \frac{v}{c} \right)^6 \left[ (k_p \cdot p'_p)(k'_p \cdot p_e) - (k_p \cdot p_p)(k'_p \cdot p'_p) \right] \Big\},
\end{aligned} \tag{2.111}$$

where  $k_e = (k, v\mathbf{k})$  is an electron four-vector and  $k_p = (k, c\mathbf{k})$  is a photon four-vector. We set the spherical coordinates with the  $z$  axis parallel to  $\mathbf{q}$  and choose the  $x$  axis so that  $\mathbf{p}$  lies in the  $zx$  plane.  $\phi$  is the azimuthal angle of  $\mathbf{k}$ . In the LLA, the scattering rates can be simplified as

$$\begin{aligned}
& \int_0^{2\pi} d\phi \sum_{\text{spins}} |\mathcal{M}_{+\text{R}, -\text{R}}^{+\text{R}, -\text{R}}(k, p, k', p')|^2 \simeq \int_0^{2\pi} d\phi \sum_{\text{spins}} |\mathcal{M}_{+\text{R}, -\text{L}}^{+\text{R}, -\text{L}}(k, p, k', p')|^2 \\
& \simeq \frac{16e^4}{\varepsilon^2} (2\pi) v^4 \frac{(pk)^2}{q^4} \left[ 1 + \frac{1}{2} \left( \frac{v}{c} \right)^4 \left( \frac{q^2 - \Omega^2}{q^2 - \left( \frac{v}{c} \right)^2 \Omega^2} \right)^2 \right].
\end{aligned} \tag{2.112}$$

As we stated before, the integral over  $q$  is logarithmically divergent. We need to introduce the upper and lower cutoffs to regularize the divergence. Here, we assume that the momentum  $q$  is small and this approximation is valid for  $q \lesssim T/v$ , i.e., the upper cutoff should be  $T/v$ . The lower cutoff is emerged from the absence of thermal self-energy insertions. This divergence will be removed by introducing higher-order perturbative corrections to the fermion self-energy, and such corrections appear at order  $\alpha$  correction. Thus, the fermion propagator without self-energy insertion is invalid for  $q \lesssim \alpha T/v$ , and the lower cutoff should be  $\alpha T/v$ . Then, the integral over  $q$  becomes

$$\int_0^\infty \frac{dq}{q} \simeq \int_{\alpha T/v}^{T/v} \frac{dq}{q} = \ln \alpha^{-1}. \tag{2.113}$$

After complicated but straightforward calculations, we finally obtain the functional  $\langle \hat{\mathbf{k}}g, \mathcal{C}[\hat{\mathbf{k}}g] \rangle$  as

$$\langle \hat{\mathbf{k}}g, \mathcal{C}[\hat{\mathbf{k}}g] \rangle = \frac{\pi N_W}{9\beta^6 v^5} (\alpha^2 \ln \alpha^{-1}) F\left(\frac{v}{c}\right) [\xi(\omega)]^2, \tag{2.114}$$

where  $\beta = 1/T$  and the function  $F(x)$  is given by

$$F(x) = 1 + \frac{1}{4} \left[ 3 - x^2 - \frac{(1 - x^2)(3 + x^2)}{x} \tanh^{-1} x \right]. \tag{2.115}$$

The function  $F(v/c)$  can be regarded as relativistic correction, and it cannot be obtained from the nonrelativistic analysis [7]. In the nonrelativistic limit ( $v/c \rightarrow 0$ ), we have  $F(v/c) = 1$ , and it monotonically increases to  $F(v/c) = 3/2$  ( $v/c \rightarrow 1$ ). From Eq. (2.114), the variational functional  $\mathcal{Q}[k\xi(\omega)]$  becomes

$$\begin{aligned}
& \mathcal{Q}[k\xi(\omega)] \\
&= \frac{1}{4\pi^2} \frac{1}{(\beta v)^5} \left\{ i\omega \frac{7\pi^4}{30} [\xi(\omega)]^2 + 9(\beta v)^2 \zeta(3) \xi(\omega) \right\} - \frac{1}{2} \frac{\pi N_W}{9\beta^6 v^5} (\alpha^2 \ln \alpha^{-1}) F\left(\frac{v}{c}\right) [\xi(\omega)]^2.
\end{aligned} \tag{2.116}$$

### 2.6.3 Solution

Now that we have the variational functional  $\mathcal{Q}[k\xi(\omega)]$ , we can determine  $\xi(\omega)$  by the functional derivative as

$$\xi(\omega) = \frac{81\zeta(3)}{4\pi^3} \beta^3 v^2 \left[ N_W (\alpha^2 \ln \alpha^{-1}) F\left(\frac{v}{c}\right) - \frac{21\pi}{20} i\beta\omega \right]^{-1}. \tag{2.117}$$

Then, the electric conductivity in the LLA is

$$\begin{aligned}
\sigma^{(N)}(\omega, T) &= e^2 v \sum_{\lambda a} \int_{\mathbf{k}} \frac{k_x^2}{k^2} \frac{1}{\beta v} \left( -\frac{\partial f_{\lambda}^0(k)}{\partial k} \right) k \xi(\omega) \\
&= \frac{3\zeta(3)}{2\pi^2} N_W \frac{e^2}{\beta^4 v^3} \xi(\omega)
\end{aligned}$$

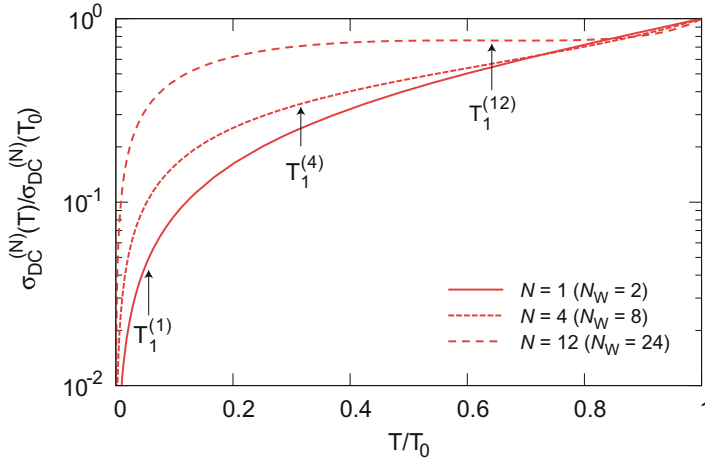


**Fig. 2.10** DC conductivity  $\sigma_{DC}^{(N)}(T)$ . The DC conductivity decreases at lower temperatures. Reprinted figure with permission from Ref. [13]. Copyright 2013 by the American Physical Society

$$= N_W \frac{e^2}{h^2} \left( \frac{k_B T}{\hbar v} \right) \frac{243[\zeta(3)]^2}{4\pi^4} \left[ N_W (\alpha^2 \ln \alpha^{-1}) F\left(\frac{v}{c}\right) - \frac{21\pi}{20} i\beta\omega \right]^{-1}. \quad (2.118)$$

$k_B$  and  $\hbar$  are recovered in the last line of the equation. Especially, the DC conductivity is

$$\sigma_{\text{DC}}^{(N)}(T) = \frac{e^2}{h} \frac{k_B T}{\hbar v} \frac{0.90}{\alpha^2 \ln \alpha^{-1} F(v/c)}, \quad (2.119)$$

and shown in Fig. 2.10.

## 2.7 Energy Gap

Up to now, we have focused on the critical point ( $m = 0$ ), but the mass  $m$  is a relevant parameter. Experimentally, the bare mass  $m_0$  can be controlled by the concentration  $x$  or by pressure  $P$  [23, 24]. The RG equation for mass  $m(\kappa)$  is [25]

$$\kappa \frac{dm(\kappa)}{d\kappa} = -\frac{3\alpha(\kappa)}{2\pi} m. \quad (2.120)$$

Then, the mass at momentum scale  $\kappa$  is

$$m(\kappa) = m(\Lambda) \left[ 1 + \frac{2N+2}{3\pi} \alpha_0 \ln \left( \frac{\Lambda}{\kappa} \right) \right]^{9/(4N+4)}. \quad (2.121)$$

When we neglect the weak singularity with  $\ln \ln m_0$ , the solution to Eq. (2.121) is given by

$$m = m_0 \left[ 1 + \frac{2N+2}{3\pi} \alpha_0 \ln \left( \frac{\Lambda}{m_0} \right) \right]^{9/(4N+4)}, \quad (2.122)$$

which describes the critical behavior of the gap as a function of  $m_0 \propto (x - x_c)$  or  $m_0 \propto (P - P_c)$  with  $x_c$  ( $P_c$ ) being the critical concentration (pressure).

## 2.8 Discussions and Summary

Now we discuss the relevance of the present results to the real systems. First, for a TI ( $N = 1$ ), the velocity  $v_0$  is estimated as  $v_0 \simeq 10^6$  m/s from the ARPES measurement of the energy dispersion [23], hence  $c_{\text{vacuum}}/v_0 \simeq 300$ . As the dielectric constant, we take the typical value  $\varepsilon_0 \simeq 10^2$  for BiSb alloys [26]. Since  $c_0 = c_{\text{vacuum}}/\sqrt{\varepsilon_0}$ ,  $c_0/v_0 \simeq 30$  and  $\alpha_0 = (1/137)/(\varepsilon v) \simeq 0.022$  are obtained. These values give the estimates for  $\kappa_1 \simeq 10^{-47} \kappa_0$  and  $\kappa_2 \ll \kappa_1$ .

For the pyrochlore iridate  $\text{Y}_2\text{Ir}_2\text{O}_7$  with  $N = 12$  ( $N_W = 24$ ), the velocity and the dielectric constant may be estimated as  $v_0 \simeq 10^6$  m/s and  $\varepsilon_0 \simeq 10$  [7]. In this case  $c_0/v_0 \simeq 95$  and  $\alpha_0 \simeq 0.22$ ; we obtain  $\kappa_1 \simeq 0.2\kappa_0$  and  $\kappa_2$  is extremely small. The value  $\kappa_1 \simeq 0.2\kappa_0$  would be physically accessible.

To experimentally observe the RG effects, we have to search materials with reasonably large  $\kappa_1$  and  $\kappa_2$ . A larger coupling constant  $\alpha_0$  is necessary to obtain larger  $\kappa_1$ , and this can be realized if both of the dielectric constant  $\varepsilon_0$  and the Fermi velocity  $v$  are small. In addition to large  $\alpha_0$ , small  $c_0/v_0$  is required to make  $\kappa_2$  larger. There seem to be two approaches: (a) small  $c_0$  and (b) large  $v_0$ . In case (a), a large dielectric constant  $\varepsilon_0$  leads to the small coupling constant  $\alpha_0$  (assuming  $\mu_0 = 1$ ), and hence it cannot be a solution. In case (b), a large  $v_0$  also brings a small  $\alpha_0$ . The only way out is the small ratio of  $c_0/v_0$ . Unfortunately, it would be difficult to observe the relativistic scaling behavior at the experimentally accessible temperature in the materials at hand.

This estimation gives a justification for the nonrelativistic approximation. Physically accessible  $\kappa_1$  is easily obtained by choosing appropriate  $v_0$  and  $\varepsilon_0$ , but it would be difficult to access  $\kappa_2$  unless  $c_0 \approx v_0$ . It means that the nonrelativistic approximation in the RG analysis is adequate in ordinary situations. However, if  $c_0 \approx v_0$  is accomplished with  $\varepsilon_0 \sim 1$  and  $\mu_0 \ll 1$ , we might reach  $\kappa_2$ , i.e., the relativistic scaling region.

In summary, we have studied the (3+1)D Dirac electrons coupled to electromagnetic field as the model for quantum critical phenomena of topological phase transition and Weyl semimetals. The RG equations are derived and the two scaling regions are identified (i.e., the nonrelativistic and relativistic scaling regions). The Lorentz invariance is recovered in the latter case. The physical properties such as the permittivity, the permeability, the electron spectral function, the conductivity, and the mass gap have been discussed based on the RG equations.

## References

1. M.E. Peskin, D.V. Schroeder, *An Introduction to Quantum Field Theory* (Westview Press, Boulder, 1995)
2. P. Ramond, *Field Theory: A Modern Primer*, 2nd edn. (Addison-Wesley, Redwood City, 1990)
3. A. Damascelli, Z. Hussain, Z.-X. Shen, *Rev. Mod. Phys.* **75**, 473 (2003)
4. V.N. Kotov, B. Uchoa, V.M. Pereira, F. Guinea, A.H. Castro Neto, *Rev. Mod. Phys.* **84**, 1067 (2012)
5. J. González, F. Guinea, M. Vozmediano, *Nucl. Phys. B* **424**, 595 (1994)
6. P. Goswami, S. Chakravarty, *Phys. Rev. Lett.* **107**, 196803 (2011)
7. P. Hosur, S.A. Parameswaran, A. Vishwanath, *Phys. Rev. Lett.* **108**, 046602 (2012)
8. B. Roy, V. Juričić, I.F. Herbut, *Phys. Rev. B* **87**, 041401 (2013)
9. R. Shindou, S. Murakami, *Phys. Rev. B* **79**, 045321 (2009)
10. X.-L. Qi, S.-C. Zhang, *Rev. Mod. Phys.* **83**, 1057 (2011)
11. G. 't Hooft, M. Veltman, *Nucl. Phys. B* **44**, 189 (1972)
12. H. Isobe, N. Nagaosa, *Phys. Rev. B* **86**, 165127 (2012)
13. H. Isobe, N. Nagaosa, *Phys. Rev. B* **87**, 205138 (2013)
14. J.C. Ward, *Phys. Rev.* **78**, 182 (1950)

15. Y. Takahashi, *Nuovo Cimento* **6**, 371 (1957)
16. C.G. Callan, *Phys. Rev. D* **2**, 1541 (1970)
17. K. Symanzik, *Commun. Math. Phys.* **18**, 227 (1970)
18. K. Symanzik, *Commun. Math. Phys.* **23**, 49 (1971)
19. S. Coleman, *Aspects of symmetry* (Cambridge University Press, Cambridge, 1988)
20. G.S. Adkins, *Phys. Rev. D* **27**, 1814 (1983)
21. P. Arnold, G.D. Moore, L.G. Yaffe, *J. High Energy Phys.* **11**, 001 (2000)
22. L. Fritz, J. Schmalian, M. Müller, S. Sachdev, *Phys. Rev. B* **78**, 085416 (2008)
23. S.-Y. Xu, Y. Xia, L.A. Wray, S. Jia, F. Meier, J.H. Dil, J. Osterwalder, B. Slomski, A. Bansil, H. Lin, R.J. Cava, M.Z. Hasan, *Science* **332**, 560 (2011)
24. T. Sato, K. Segawa, K. Kosaka, S. Souma, K. Nakayama, K. Eto, T. Minami, Y. Ando, T. Takahashi, *Nat. Phys.* **7**, 840 (2011)
25. L.S. Brown, *Quantum Field Theory* (Cambridge University Press, Cambridge, 1992)
26. X.-L. Qi, R. Li, J. Zang, S.-C. Zhang, *Science* **323**, 1184 (2009)

Theoretical Study on Correlation Effects in Topological  
Matter

Isobe, H.

2017, XII, 136 p. 46 illus., 41 illus. in color., Hardcover

ISBN: 978-981-10-3742-9